# Angular-resolved linear and circular dichroism in core-level photoemission of metallic systems

Gerrit van der Laan
*Daresbury Laboratory, Warrington WA4 4AD, United Kingdom*
(Received 22 April 1994; revised manuscript received 25 August 1994)

Angle-dependent core-level photoemission excited with polarized x rays can be used to determine the magnetic properties of metallic systems by separating the geometrical dependence from the physical information that is contained in the spectra. There are four different geometries which can be distinguished: magnetic circular dichroism, linear dichroism, circular dichroism in the angular dependence, and magnetic linear dichroism in the angular dependence. The shape of the dichroic spectra in a one-electron model is determined by the core spin-orbit interaction and the spin field. A good agreement between experiment and theory is obtained for the Fe $3p$ photoemission of iron when the spin and orbit dependence of the lifetime broadening is taken into account. The influence of the orbit field and the spin filtering in the solid can be estimated from the first spectral moment.

## I. INTRODUCTION

In the last two decades angle-resolved photoemission has developed into a useful method to study the electronic structure of solids. Specific information about the symmetry and the hybridization can be obtained from the multiplet splitting and satellite structure in core levels. With the advent of polarized x rays from synchrotron-radiation sources, a surprisingly strong magnetic dichroism was discovered in core-level photoemission.[1–11] Schneider, Venus, and Kirschner[1] have observed a magnetic circular dichroism in the angle-dependent photoemission of the Fe $2p$ level which does not disappear when the magnetization direction is perpendicular to the helicity vector of the light. This is in contrast with the findings for the circular dichroism in x-ray absorption. Even more remarkable was the observation by Roth *et al.*[2] that the Fe $3p$ photoemission signal taken with linearly polarized light changes upon reversal of the magnetization direction which is perpendicular to the plane containing the directions of the light polarization and the electron emission. The latter effect is different from linear dichroism which measures the quadrupole moment.[3] Although dichroism experiments have been explained qualitatively,[1–4,11–15] the physical information contained in these spectra has not yet been fully analyzed.

In a series of three papers[16–18] (Papers I, II, and III), Thole and van der Laan have given a general theory for spin polarization and magnetic dichroism in photoemission from core and valence states in localized magnetic systems. In Paper I the origin of the spin polarization and magnetic dichroism was discussed. The different ways to orient the polarizations of the magnetization, electric vector of the light, and the spin of the photoelectron allow measurements of different kinds of correlations between the corresponding atomic properties: the valence spin, core hole orbital momentum, and core hole spin, respectively. The fundamental spectra can be defined as those linear combinations of the polarized spectra that are directly connected to physical properties. They are the natural quantities to obtain the information about the many-electron system contained in the spectrum.

In Paper II it was shown that for the emission from an incompletely filled localized shell, such as the $4f$ shell in the rare earths, the integrated intensities of the magnetic circular dichroism and spin spectrum are proportional to the ground-state orbital and spin magnetic moment, respectively. In Paper III the angular dependence was analyzed. The geometry can be separated from the physical properties and the angular dependence provides a way to measure higher magnetic moments. The interference term between the $l-1$ and $l+1$ emission channels allows one to measure the odd magnetic moments with linearly polarized light. In angle-integrated photoemission these magnetic moments can only be measured with circularly polarized light.

In this paper we will extend the theory to metallic systems. We will analyze the dichroism within a one-electron model which will make simple and accurate calculations possible under many circumstances. We will explain the observed dichroism in the angular dependent emission from ferromagnetic iron.

The origin of core-level polarization can be understood when we consider a core level $l$ which is split into sublevels with orbital component $m$. In an atomic model this splitting is caused by the electrostatic interaction of the core level with the magnetically polarized valence electrons. In the one-electron model we assume that this splitting occurs by a spin field in combination with spin-orbit interaction. The sublevels $m$ can also be split by an orbit field, which in an atomic model is due to the correlation of the valence spin and the core orbital moment by valence spin-orbit interaction and core-valence interaction.[16]

The photoemission from each sublevel to the continuum has a different dipole transition probability for left- ($\Delta m=-1$) and right- ($\Delta m=+1$) circularly polarized radiation. E.g., for emission from an $m=l$ sublevel to the continuum state $c=l-1$ with components $\gamma$, where $-l+1\leq\gamma\leq l-1$, the transition $\Delta m=-1$ is allowed, but

 

the transition $\Delta m=+1$ is forbidden. Thus we observe a circular dichroism if the different $m$ components are resolved in energy. We can also distinguish between the $\gamma$ components of the photoelectron, since they have a different angular dependence. The core-level dichroism can be used as a probe of the magnetic properties by separating the information about the $m$ levels, which is the physical information we are interested in, from the angular part, which is simply determined by the known directions of the magnetization, the polarization vector of the light, and the emission of the photoelectron.

In Sec. II we provide an expression for the angular dependence which gives us the relations for the photoemission from a $p$ core level in the different geometries. We indicate the various ways in which the linear and circular dichroism can be obtained. In Sec. III the influence of the different interactions on the spectral shape is examined. The Fe $2p$ and $3p$ photoemission spectra are calculated and compared with reported measurements. In Sec. IV the conclusions are drawn.

## II. ANGULAR DEPENDENCE

In cylindrical symmetry the general expression of the angular-dependent photoemission $J^a$ in the direction $\varepsilon$ for light specified by the moment $a$ and polarization $\mathbf{P}$ from an atom with a magnetic multipole along the direction $\mathbf{M}$ is given as[18]

$$J^a(\mathbf{P},\varepsilon,\mathbf{M})=\frac{1}{4\pi}\sum_x I^x \sum_b U^{abx}(\mathbf{P},\varepsilon,\mathbf{M}) \times \sum_{cc'} A^{cc'}_{abx} R^c R^{c'} e^{i(\delta_c-\delta_{c'})} , \quad (1)$$

where $R^c$ is the radial dipole matrix element and $\delta_c$ is the phase shift for excitation to the continuum state with orbital momentum $c=l\pm1$, and where we allow for interference between the two final-state channels $c$ and $c'$. The $I^x$ gives the spectral intensity. Each $I^x$ produces a limited set of angular distributions ("waves") $U^{abx}$ with contributions from each channel as a numerical factor $A$ times the radial matrix elements and phase shifts, where $a$, $b$, and $x$ are the moments of the light, the photoelectron distribution, and the atomic shell, respectively. In this notation $a=0$ means isotropic light, i.e., the sum of intensities obtained with right-circularly ($q=-\Delta m=-1$), $Z$-linearly ($q=-\Delta m=0$), and left-circularly ($q=-\Delta m=+1$) polarized radiation. For isotropic light the polarization $\mathbf{P}$ has no meaning. By $a=1$ we denote circular dichroism: the difference in intensities for left- and right-circularly polarized light with the helicity vector along $\mathbf{P}$. By $a=2$ we denote linear dichroism: the intensities for light polarized in two perpendicular directions perpendicular to $\mathbf{P}$ ($q=1$ and $-1$) minus twice the intensity for light polarized along $\mathbf{P}$ ($q=0$).

The spectra $I^x$ give the probability for removing an electron with moment $x$. Since there are $2l+1$ orbital components in the core shell, we have that $x=0,\ldots,2l$. The spectra $I^x$ are a function of the final state $|f\rangle$ and can be written as a function of photon energy $\omega$, photoelectron energy $E$, and initial and final-state energies $E_g$ and $E_f$ using

$$I^x(E,\omega)=\sum_f I^x(f)\delta(E+E_f-\omega-E_g) . \quad (2)$$

These spectra do not include the radial integrals which appear separately in Eq. (1). The intensities $I^x(f)$ of the one-electron state final states are given as[19]

$$I^x(f)\equiv n_{lx}^{-1}\left\langle (-)^{l-m}\begin{bmatrix} l & x & l \\ -m & 0 & m\end{bmatrix}\right\rangle , \quad (3)$$

where the numerical factor

$$n_{lx}\equiv\begin{bmatrix} l & x & l \\ -l & 0 & l\end{bmatrix}=\frac{(2l)!}{\sqrt{(2l-x)!(2l+1+x)!}} , \quad (4)$$

has been used to remove the square roots. The angular brackets in Eq. (3) mean that the expectation value has to be taken over the enclosed expression. The symbols with the parentheses are 3-$j$ symbols, which can be worked out for each value of $x$, e.g.,

$$I^0(f)=1 , \quad (5)$$

$$I^1(f)=\langle m\rangle l^{-1} , \quad (6)$$

$$I^2(f)=[\langle m^2\rangle-\tfrac{1}{3}l(l+1)][\tfrac{1}{3}l(2l-1)]^{-1} . \quad (7)$$

The integrated intensity of the $I^0$ spectrum is $4l+2$, which is the number of core electrons. The integrated intensities of the $I^{x\neq0}$ spectra are zero.

The $I^0$ spectrum is independent of the external field. The other spectra require an external field, i.e., Coulomb and/or exchange interaction to correlate the moment of the core electron with the magnetic multipole moment of the valence electrons. An odd value of $x$ involves an oriented magnetic moment (dipole, octupole, etc.) and an even value of $x$ involves a (magnetically or electrostatically) aligned moment (quadrupole or hexadecapole, etc.) For a one-electron model the situation is schematically drawn in Fig. 1, where spin-orbit interaction $\zeta$ (dotted line), an orbit field $H_l$, and spin field $H_s$ (dashed lines)

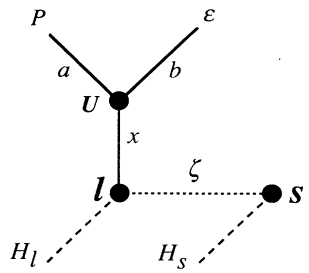


FIG. 1. Schematic one-electron picture for the angular dependence in polarized photoemission with spin-orbit interaction $\zeta$ (dotted line) and an orbit field $H_l$ and spin field $H_s$ (dashed lines) along $\mathbf{M}$ acting on the orbit $l$ and spin $s$ of the electron. The light polarization $\mathbf{P}$, the photoelectron direction $\varepsilon$, and the orbit have moments $a$, $b$, and $x$, respectively. The moment $x$ is induced either by the orbit field $H_l$, or by the spin field $H_s$ together with spin-orbit interaction $\zeta$. The angular dependence is given by the function $U^{abx}(\mathbf{P},\varepsilon,\mathbf{M})$.

TABLE I. Angle-dependent functions $U^{abx}(\mathbf{P},\varepsilon,\mathbf{M})$.

$U^{000}=1$
$U^{022}=\frac{3}{2}(\varepsilon\cdot\mathbf{M})^2-\frac{1}{2}$
$U^{101}=\mathbf{P}\cdot\mathbf{M}$
$U^{121}=\frac{3}{2}(\mathbf{P}\cdot\varepsilon)(\varepsilon\cdot\mathbf{M})-\frac{1}{2}(\mathbf{P}\cdot\mathbf{M})$
$U^{122}=\frac{6}{5}(\varepsilon\cdot\mathbf{M})\mathbf{P}\cdot(\varepsilon\times\mathbf{M})$
$U^{220}=\frac{3}{2}(\mathbf{P}\cdot\varepsilon)^2-\frac{1}{2}$
$U^{221}=\frac{6}{5}(\mathbf{P}\cdot\varepsilon)\mathbf{P}\cdot(\varepsilon\times\mathbf{M})$
$U^{202}=\frac{3}{2}(\mathbf{P}\cdot\mathbf{M})^2-\frac{1}{2}$
$U^{222}=\frac{1}{2}[2-3(\varepsilon\cdot\mathbf{M})^2-3(\mathbf{P}\cdot\mathbf{M})^2-3(\mathbf{P}\cdot\varepsilon)^2+9(\mathbf{P}\cdot\varepsilon)(\varepsilon\cdot\mathbf{M})(\mathbf{P}\cdot\mathbf{M})]$
$U^{242}=\frac{1}{8}[1-5(\varepsilon\cdot\mathbf{M})^2+2(\mathbf{P}\cdot\mathbf{M})^2-5(\mathbf{P}\cdot\varepsilon)^2-20(\mathbf{P}\cdot\varepsilon)(\varepsilon\cdot\mathbf{M})(\mathbf{P}\cdot\mathbf{M})+35(\mathbf{P}\cdot\varepsilon)^2(\varepsilon\cdot\mathbf{M})^2]$

along $\mathbf{M}$ act on the orbit $l$ and spin $s$ of the electron. The $I^1$ spectrum can be observed if the sublevels $m$ are split by a spin field $H_s$ together with spin-orbit interaction. An odd orbit field $H_l$ will also split the $m$ levels, but such a field will usually be small in $3d$ transition metals. Observation of the $I^2$ spectrum requires a splitting of the sublevels with different values of $|m|$ by either an (even) electrostatic field $H_l$ or by a magnetic alignment $H_s$ along $\mathbf{M}$ together with spin-orbit interaction.

The angular-dependent functions in Eq. (1) are defined as

$$U^{abx}(\mathbf{P},\varepsilon,\mathbf{M}) \equiv \sum_{\alpha} \underline{n}_{abx}^{-1} \begin{bmatrix} a & b & x \\ -\alpha & \alpha & 0 \end{bmatrix} C^a_{\alpha}(\mathbf{P}) C^b_{-\alpha}(\varepsilon) C^x_0(\mathbf{M}) , \quad (8)$$

where

$$C^k_{\kappa}(\theta,\varphi)=\left[\frac{4\pi}{2k+1}\right]^{1/2} Y^k_{\kappa}(\theta,\varphi) , \quad (9)$$

are normalized spherical harmonics and $\underline{n}_{abx}^{-1}$ is a normalization constant.[18] Table I gives the angle-dependent functions for $l=1$ with values of $abx$ which are allowed by parity and momentum conservation.

The moment $b$ of the photoemission distribution must be even due to parity symmetry. Conservation of the angular momentum gives the triangular condition $b=|a-x|,\ldots,a+x$. Thus in angle-integrated emission where $b=0$ we have that $a=x$, so that the measured circular dichroism $J^1$ is proportional to the $I^1$ spectrum [cf. Eq. (16)] and the linear dichroism $J^2$ is proportional to the $I^2$ spectrum [c.f. Eq. (17)]. The moment $b=2$ corresponds to an emission distribution with the shape of a $d$-wave function (see, e.g., Figs. 2 and 3). This moment allows us to measure $I^1$ both in circular dichroism ($abx=121$) as well as in linear dichroism ($abx=221$). Likewise, $I^2$ can be measured in circular dichroism ($abx=122$) as well as in linear dichroism ($abx=222$). For a $p$ core shell we have $x=0,1,2$ which limits $b$ to 0,2,4. A more complicated situation arises for a $d$ core shell where $x=0,\ldots,4$.[18] Then depending on the geometry $J^1$ and $J^2$ will measure either a combination of $I^1$ and $I^3$ or a combination of $I^2$ and $I^4$. Thus the emission from a $p$ core shell is a relatively simple case.

Substituting the values of $A$ given in Table II, we can write out $J^a(\mathbf{P},\varepsilon,\mathbf{M})$ for a $p$ level as

$$4\pi J^0=I^0U^{000}(\tfrac{1}{3}R^{00}+\tfrac{2}{3}R^{22})+I^2U^{022}[-\tfrac{1}{3}(R^{02}+R^{20})-\tfrac{1}{3}R^{22}] , \quad (10)$$

$$4\pi J^1=I^1\{U^{101}(\tfrac{1}{3}R^{00}-\tfrac{1}{3}R^{22})+U^{121}[-\tfrac{1}{3}(R^{02}+R^{20})+\tfrac{2}{3}R^{22}]\}+I^2U^{122}\tfrac{5}{12}i(R^{02}-R^{20}) , \quad (11)$$

$$4\pi J^2=I^0U^{220}[-\tfrac{2}{3}(R^{02}+R^{20})-\tfrac{2}{3}R^{22}]+I^1U^{221}\tfrac{5}{4}i(R^{02}-R^{20}) +I^2\{U^{202}(\tfrac{1}{3}R^{00}+\tfrac{1}{15}R^{22})+U^{222}[\tfrac{1}{3}(R^{02}+R^{20})-\tfrac{2}{21}R^{22}]+U^{242}\tfrac{36}{35}R^{22}\} , \quad (12)$$

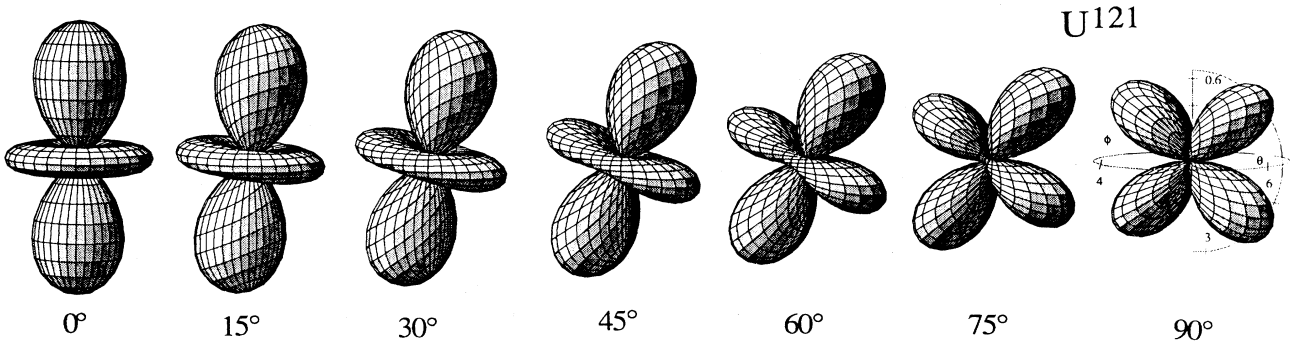


FIG. 2. The bipolar spherical harmonic $U^{121}$ for different values of $\theta_1=\angle(\mathbf{M},\mathbf{P})$ as indicated in degrees ($\phi_1=0°$). $\mathbf{M}$ is always along the positive $z$ axis.

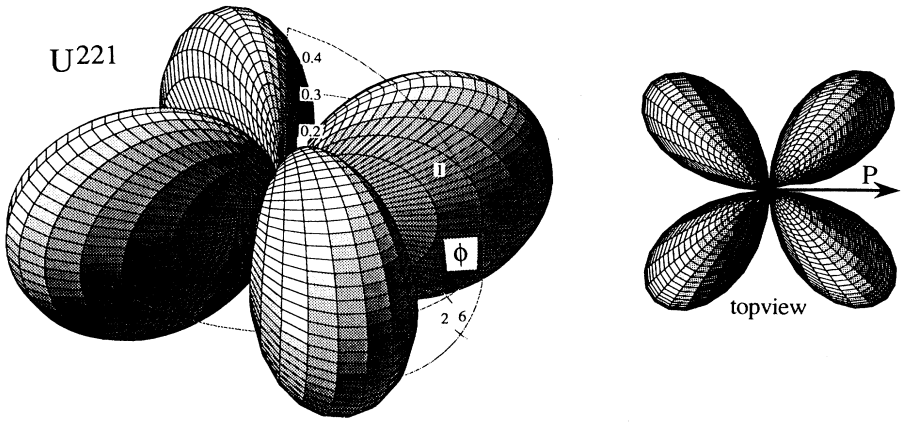


FIG. 3 The bipolar spherical harmonic $U^{221}$ for $\mathbf{M}\perp\mathbf{P}$. The maximum signal is at $\angle(\varepsilon,\mathbf{P})=45°$ and 135°. $\mathbf{M}$ is along the positive $z$ axis. The lobes have alternately positive and negative intensities.

where $R^{20}=R^0R^2e^{i\delta}$ and $R^{02}=R^0R^2e^{-i\delta}$ with phase difference $\delta\equiv\delta_0-\delta_2$. The interference terms in Eqs. (10)–(12) are of special interest and can be written as

$$R^{20}+R^{02}=R^0R^2(e^{i\delta}+e^{-i\delta})=2R^0R^2\cos\delta\ , \tag{13}$$

$$R^{20}-R^{02}=R^0R^2(e^{i\delta}-e^{-i\delta})=2iR^0R^2\sin\delta\ . \tag{14}$$

Inspection of Eqs. (11) and (12) shows that the interference term given in Eq. (14) only occurs for $a+b+x=$odd. Since $b$ is even, either one of the other moments, say $a$, must be odd. Then the intensity must be zero in a coplanar geometry. This is so because inverting $a$ gives a change of sign, but the same geometry can be obtained by inverting $b$ and $x$, which are even and give no sign change. Therefore $U=-U=0$. This can also be seen from Table I where the odd waves contain a factor $\mathbf{P}\cdot\varepsilon\times\mathbf{M}$ which is zero in planar geometry. Thus waves with $a+b+x=$odd can only be measured when the geometry, which is spanned by $\mathbf{P}$, $\varepsilon$, and $\mathbf{M}$ has no inversion symmetry (i.e., is not coplanar), in which case we will call it a chiral geometry.

$U^{abx}$ changes sign whenever one of the vectors corresponding to an odd moment $a$ or $x$ is inverted. The intensity of an odd wave with two even moments is zero when one of the even moments is perpendicular to the other two moments. This is because inversion of the odd moment, which gives a sign change, followed by a rotation leads to the same geometry as inversion of the two even moments, which gives no sign change.

The integral of the $U^{abx}$ over all $\varepsilon$ is zero whenever $b\neq0$. The angle-integrated intensities are obtained from the terms with $b=0$ in Eqs. (10)–(12) as

$$J_t^0=\tfrac{1}{3}I^0(R^{00}+2R^{22})\ , \tag{15}$$

$$J_t^1=\tfrac{1}{3}I^1\mathbf{P}\cdot\mathbf{M}(R^{00}-R^{22})\ , \tag{16}$$

$$J_t^2=\tfrac{1}{6}I^2[3(\mathbf{P}\cdot\mathbf{M})^2-1](R^{00}+\tfrac{1}{5}R^{22})\ , \tag{17}$$

where the interference terms have disappeared. It is clear that for each $J_t^a$ the two final-state channels have different coefficients.

In angular-dependent photoemission $I^1$ and $I^2$ can be measured using either linear or circular dichroism. This results in the four different types of geometries which are summarized in Table III. In the first one, which was first used by Baumgarten *et al.*,[4] the $I^1$ spectrum is measured in circular dichroism ($a=1$) and since an odd magnetic moment is required it is called magnetic circular dichroism (MCD). From Eq. (11) we obtain

TABLE II. The nonzero values of $A_{abx}^{cc'}$ for $p$ photoemission.

| $abx$ | $cc'=00$ | $cc'=20$ | $cc'=22$ |
|---|---|---|---|
| 000 | $\frac{1}{3}$ | | $\frac{2}{3}$ |
| 022 | | $-\frac{1}{3}$ | $-\frac{1}{3}$ |
| 101 | $\frac{1}{3}$ | | $-\frac{1}{3}$ |
| 121 | | $-\frac{1}{3}$ | $\frac{2}{3}$ |
| 122 | | $\frac{5}{12}i$ | |
| 202 | $\frac{1}{3}$ | | $\frac{1}{15}$ |
| 220 | | $-\frac{2}{3}$ | $-\frac{2}{3}$ |
| 221 | | $\frac{5}{4}i$ | |
| 222 | | $\frac{1}{3}$ | $-\frac{2}{21}$ |
| 242 | | | $\frac{36}{35}$ |

TABLE III. The four types of geometries with their spectra, symmetry properties, and angle-dependent factors for $p$ emission. The acronyms make clear under which conditions the spectra can be measured. In circular dichroism (CD) we measure the difference between the two circular polarizations of the light ($a=1$). In linear dichroism (LD) we measure the difference between two orthogonal linear polarizations ($a=2$). The spectra with prefix M can also be obtained by reversing the magnetic moment ($x=$odd). Alternatively, MCD and LD can be referred to as MCDAD and LDAD, respectively, but here we reserve the postfix AD for the case that the measurement requires interference between the two channels, and therefore a chiral geometry ($a+b+x=$odd).

| Acronym | $J^a$ | $I^x$ | $a+b+x$ | $U^{abx}$ |
|---|---|---|---|---|
| MCD | $J^1$ | $I^1$ | Even | $U^{101}+U^{121}$ |
| CDAD | $J^1$ | $I^2$ | Odd | $U^{122}$ |
| MLDAD | $J^2$ | $I^1$ | Odd | $U^{221}$ |
| LD | $J^2$ | $I^2$ | Even | $U^{202}+U^{222}+U^{242}$ |

$$J_{\mathrm{MCD}} \equiv J^1(\mathrm{even}) = \frac{1}{12\pi} I^1 [U^{101}(R^{00} - R^{22}) + 2U^{121}(R^{22} - R^0 R^2 \cos\delta)]$$

$$= \frac{1}{12\pi} I^1 \{\mathbf{P}\cdot\mathbf{M}(R^{00} - R^{22}) + [3(\mathbf{P}\cdot\varepsilon)(\varepsilon\cdot\mathbf{M}) - \mathbf{P}\cdot\mathbf{M}](R^{22} - R^0 R^2 \cos\delta)\} , \quad (18)$$

where even means that only even waves are considered. The last form of the expression shows more clearly the angular distribution. $U^{101} = \mathbf{P}\cdot\mathbf{M}$ is the angle-independent emission distribution ($b = 0$) [cf. Eq. (16)], which is spherical for any given $\theta_1 = \angle(\mathbf{M},\mathbf{P})$. The function $U^{121} = \frac{3}{2}(\mathbf{P}\cdot\varepsilon)(\varepsilon\cdot\mathbf{M}) - \frac{1}{2}(\mathbf{P}\cdot\mathbf{M})$ gives the angular dependence of the emission ($b \neq 0$), which is zero integrated over all emission angles. Since $b \leq c + c'$ only the $d$ continuum ($c = c' = 2$) and the interference term($c = 2, c' = 0$) can have a $U^{121}$ dependence. This function is plotted in Fig. 2 for different values of $\theta_1$ and taking $\mathbf{M} \| z$. This shape changes from a $d(z^2)$ function for $P \| z$ ($\theta_1 = \phi = 0°$) to a $d(xz)$ function for $\mathbf{P} \| x$ ($\theta_1 = 90°$, $\phi = 0°$), where the doughnut of negative intensity has changed into a lobe along the bisectrix of the $x$ and $z$ axes. The maximum of the emission is along the bisectrix of $\angle\mathbf{P},\mathbf{M}$. As was also experimentally observed[4] the angular-dependent emission $U^{121}$ does not vanish when $\mathbf{M} \perp \mathbf{P}$, although $U^{101}$ is zero.

The $I^1$ spectrum can also be measured in linear dichroism ($a = 2$). From Eq. (12) we obtain

$$J_{\mathrm{MLDAD}} \equiv J^2(\mathrm{odd}) = \frac{3}{4\pi} I^1 \mathbf{P}\cdot(\varepsilon \times \mathbf{M})(\mathbf{P}\cdot\varepsilon) R^0 R^2 \sin\delta , \quad (19)$$

which is called the magnetic linear dichroism in the angular dependence (MLDAD). Observation of this term requires a chiral geometry. The effect is zero in coplanar and completely orthogonal geometries. E.g., for $\mathbf{M} \perp \mathbf{P}$ and $\mathbf{M} \perp \varepsilon$ the angle dependence is proportional to $\sin 2\gamma$, where $\gamma \equiv \angle(\varepsilon,\mathbf{P})$ and the maximum signal will be observed at $\gamma = 45°$ and 135°. This can be seen from Fig. 3 where the function $U^{221} = \frac{6}{5}\mathbf{P}\cdot(\varepsilon \times \mathbf{M})(\mathbf{P}\cdot\varepsilon)$ is plotted for $\mathbf{M} \perp \mathbf{P}$.

The expression for the $I^2$ spectrum measured in linear dichroism (LD) is more lengthy and we give here only the expression for $s$-polarized light as in the measurement by Roth *et al.*,[3] where $\varepsilon \perp \mathbf{P}$, $\varepsilon \perp M$, and $\mathbf{P} \| \mathbf{M}$. From Eq. (12) we obtain

$$J_{\mathrm{LD}}(s\text{-pol}) \equiv J^2(\mathrm{even}, s\text{-pol})$$

$$= \frac{1}{24\pi} I^2 (2R^{00} + 3R^{22} - 2R^0 R^2 \cos\delta) . \quad (20)$$

The $I^2$ spectrum measured in circular dichroism is obtained from Eq. (11) as

$$J_{\mathrm{CDAD}} \equiv J^1(\mathrm{odd}) = \frac{1}{4\pi} I^2 (\varepsilon\cdot\mathbf{M})\mathbf{P}\cdot(\varepsilon \times \mathbf{M}) R^0 R^2 \sin\delta , \quad (21)$$

which is the circular dichroism in the angular dependence (CDAD) and requires a chiral geometry. For $\mathbf{P} \perp \mathbf{M}$ and $\mathbf{P} \perp \varepsilon$ the angle dependence is proportional to $\sin 2\alpha$, where $\alpha \equiv \angle(\varepsilon,\mathbf{M})$.

The physical part ($I^x$) can be separated from the geometry most easily when the radial integrals and phase factors are constant over the energy range of the spectrum ($\approx 20$ eV), which is a good assumption not too near the emission threshold or in constant final-state spectroscopy. Figure 4 shows the energy dependence of the MLDAD and MCD obtained using the values of $R$ and $\delta$ for iron calculated with Cowan's atomic Hartree-Fock program.[20] The MLDAD is large around a kinetic energy (= photon energy minus binding energy) of 25 eV, where the two matrix elements in the interference term have comparable magnitudes. The signal is zero when $\sin\delta = 0$, which is around 600 eV. The angle-integrated MCD is zero around 25 eV where the transition probabilities to the two final-state channels cancel each other.

The possibility to measure $I^1$ in interference is of great practical value because the linearly polarized radiation from a synchrotron source can be obtained with much higher intensity and purity than the circularly polarized radiation. Figure 4 shows that the interference term is also present at $\sim 1.5$ keV, so that chiral effects can even be measured using "unpolarized" radiation (which is partially linearly polarized) from a conventional Al or Mg $K\alpha$ source, as has been demonstrated by Hillebrecht and Herberg.[5]

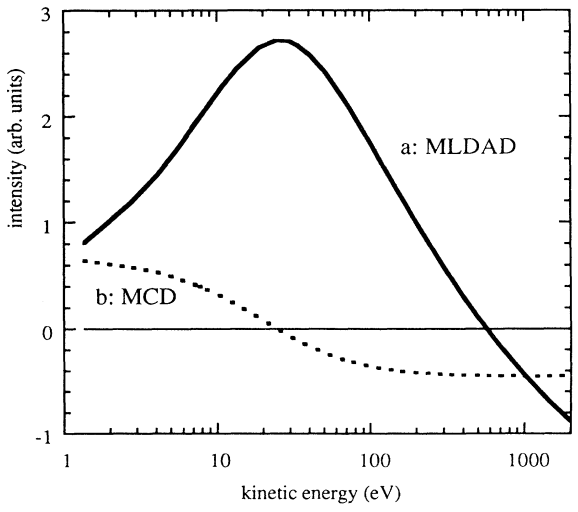


FIG. 4. The kinetic energy dependence of the Fe $3p$ photoemission signal for (a) MLDAD: $9R^0R^2\sin\delta/(R^{00} + 2R^{22})$ (solid line) and (b) angle-averaged MCD: $(R^{00} - R^{22})/(R^{00} + 2R^{22})$ (dotted line).

## III. SPECTRAL PROPERTIES

### A. Calculational details

The spectra $I^x$ contain the physical information about the magnetic system. They depend on the interactions with the valence electrons, which in a one-electron model are described by a spin-dependent field.[21]

Consider a core level which is split by spin-orbit interaction with parameter $\zeta$ and a spin field $H_s$. Figure 5 shows the energy positions of the sublevels as a function of $H_s$ (in units of $\zeta$) for a core $p$ shell. When $H_s=0$ the core level is split into a $^2P_{3/2}$ and a $^2P_{1/2}$ state which have relative binding energies of $-\zeta/2$ and $\zeta$, respectively. For $H_s/\zeta \ll 1$ both the $j=\frac{3}{2}$ and $\frac{1}{2}$ level are split into $2j+1$ sublevels which have an energy spacing of $H_s/3$ as given by the Landé interval rule. The $j=\frac{3}{2}$ contains four sublevels and the $j=\frac{1}{2}$ two sublevels. The energy sequence of these sublevels is $m_j=-\frac{3}{2},-\frac{1}{2},\frac{1}{2},\frac{3}{2}$ for the $j=\frac{3}{2}$, but $m_j=\frac{1}{2},-\frac{1}{2}$ for the $j=\frac{3}{2}$ level.

When $\zeta_p=0$ the spin field splits the $^2P$ level into a spin-down and a spin-up state with an energy separation of $H_s$. For $H_s/\zeta \gg 1$ both these states are split into three sublevels which have an energy spacing of $\zeta/2$. The energy sequence is $m=-1,0,+1$ for the spin-down state, but reversed for the spin-up state. Spin-orbit interaction mixes states with the same $m_j$ value. Since the $m_j=\pm 3/2$ are pure spin-orbit states (Table IV), they do not mix and their energy separation is equal to $H_s$. In the intermediate region where $H_s/\zeta \approx 1$, the sublevel $m_j=\frac{3}{2}$ ($=1\uparrow$) gradually migrates to the other side.

In the following we discuss the cases $H_s/\zeta=0.1$, 1.37, and 10. The first ratio is near the limit of $jj$ coupling, while the last one is near the limit of $LS$ coupling. The first two ratios represent the situation of the Fe $2p$ and $3p$ core level, respectively. Core-level photoemission spectra have been obtained using Eq. (3), where the eigenvalues and the orbital and spin components have been calculated in intermediate coupling using Cowan's code.[20] For ferromagnetic iron metal we used for the spin-orbit interaction at Hartree-Fock values of $\zeta_{2p}=8.2$ (Ref. 22) and $\zeta_{3p}=0.95$ eV (Ref. 23) and for the spin field the values of $H_s(2p)=0.8$ and $H_s(3p)=1.3$ eV obtained by solving the spin-polarized Dirac equation.[21]

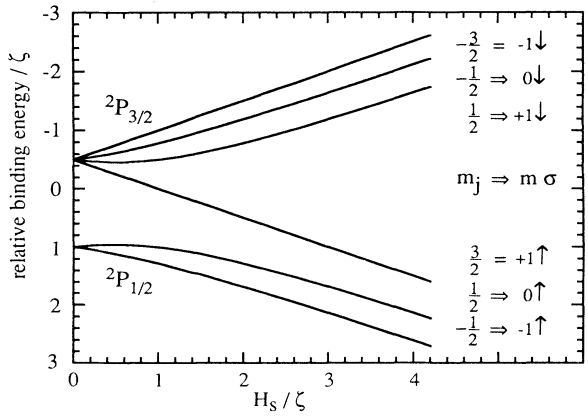


FIG. 5. Energy positions of the core $p$ sublevels as a function of the spin field $H_s$ in units of the spin-orbit parameter $\zeta$.

TABLE IV. The $jm_j$ sublevel states of a $p$ core level given as $m\sigma$ states in $jj$ and $LS$ coupling limit.

| $j$ | $m_j$ | $jj$ | $LS$ |
|---|---|---|---|
| $\frac{3}{2}$ | $-\frac{3}{2}$ | $(-1)\downarrow$ | $(-1)\downarrow$ |
| | $-\frac{1}{2}$ | $(\frac{2}{3})^{1/2}0\downarrow+(\frac{1}{3})^{1/2}(-1)\uparrow$ | $0\downarrow$ |
| | $\frac{1}{2}$ | $(\frac{1}{3})^{1/2}1\downarrow+(\frac{2}{3})^{1/2}0\uparrow$ | $1\downarrow$ |
| | $\frac{3}{2}$ | $1\uparrow$ | $1\uparrow$ |
| $\frac{1}{2}$ | $\frac{1}{2}$ | $(\frac{2}{3})^{1/2}1\downarrow-(\frac{1}{3})^{1/2}0\uparrow$ | $0\uparrow$ |
| | $-\frac{1}{2}$ | $(\frac{1}{3})^{1/2}0\downarrow-(\frac{2}{3})^{1/2}(-1)\uparrow$ | $(-1)\uparrow$ |

### B. Strong spin-orbit coupling

The spectra of the Fe $2p$ level are shown in Fig. 6 where the energy positions and intensities of the sublevels are given by the vertical lines. The curves are obtained by a convolution with a Lorentzian of $\Gamma=1$ eV to include the core hole lifetime broadening and the experimental resolution. The $I^0$ spectrum displays two peaks with a ratio of 2:1. Both peaks have dominantly spin-up character at the high binding-energy side and spin-down character at the low binding-energy side. In the $j=\frac{3}{2}$ peak the

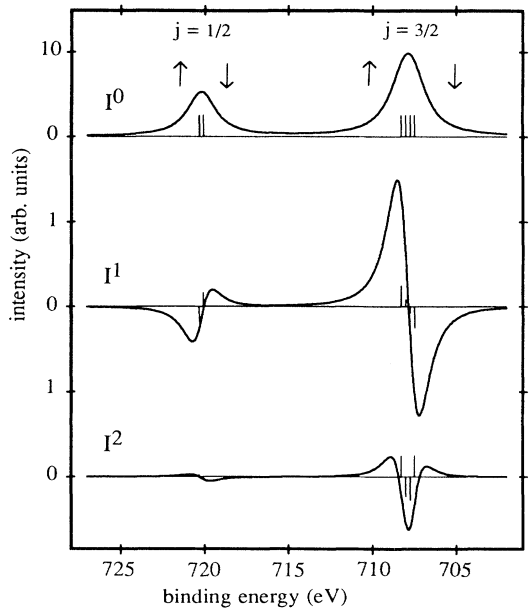


FIG. 6. Calculated $I^x$ spectra of Fe $2p$ photoemission. The spectral weight given by the vertical lines has been convoluted with a Lorentzian of $\Gamma=1$ eV. The spin preference is indicated by the up and down arrows.

spin and the orbit are coupled parallel so that orbital moment is positive at the high and negative at the low binding-energy side. This is reversed in the $j=\frac{1}{2}$ peak since the spin and the orbit are coupled antiparallel. This explains the $-+$ and $+-$ structures of the $j=\frac{1}{2}$ and $\frac{3}{2}$ peak in the $I^1$ spectrum, which is proportional to $\langle m \rangle$ [c.f. Eq. (6)]. The dichroism in the $j=\frac{3}{2}$ peak is larger than in the $j=\frac{1}{2}$ because the $m_j=\pm\frac{3}{2}$ are pure $m=\pm1$ states, whereas the $m_j=\pm\frac{1}{2}$ are mixed $m=\pm1,0$ states (Table IV). Near the limit of $jj$ coupling the $j=\frac{3}{2}$ to $j=\frac{1}{2}$ signal ratio is 5:$-$1. However, the first spectral moment of the total spectrum must remain zero (cf. Sec. III E). This is achieved by a transfer of spectral weight between the $j=\frac{3}{2}$ and $j=\frac{1}{2}$ structures, which is clearly visible in Fig. 6.

In the $I^2$ spectrum the signal for each sublevel is proportional to the value of $\langle m^2 \rangle - \frac{1}{3}l(l+1)$. Thus the spectrum can be observed if the $m_j=\pm\frac{3}{2}$ and $m_j=\pm\frac{1}{2}$ sublevels have different binding energies. The signals of the $m_j=\pm\frac{1}{2}$ and $\pm\frac{3}{2}$ sublevels have opposite signs in the $j=\frac{3}{2}$ level, which results in a structure with a $+-+$ shape. A pure $j=\frac{1}{2}$ level cannot contain an $x=2$ moment, i.e., there are only $m_j=\pm\frac{1}{2}$ sublevels, and the presence of the weak signal in Fig. 6 is due to the mixing with the $j=\frac{3}{2}$ level by the spin field.

In first-order the magnitude of the dichroism for each $j$ level is proportional to $H_s$. This is because the energy spacing is proportional to $H_s$, while $\langle m \rangle$ and $\langle m^2 \rangle$ change only in higher order.

### C. Strong spin field

The spectra for $H_s/\zeta=10$ are shown in Fig. 7. The $I^0$ spectrum consists of two peaks with equal intensity. The $I^1$ spectrum has a $-+$ and $+-$ structure for the spin-up and spin-down peak, respectively, due to the relative energy positions of the $m=-1,+1$ and $+1,-1$ sublevels. In the $I^2$ spectrum the signal is equal to the normalized value of $\langle m^2 \rangle - \frac{1}{3}l(l+1)$ of each sublevel, which for pure $m=+1,0,-1$ sublevels is $1,-2$ and 1, respectively. This causes the two $+-+$ structures. In first-order the magnitude of the dichroism for each spin state is proportional to $\zeta$, because the energy spacing is proportional to $\zeta$, while the signals change only in higher order. The $I^1$ and $I^2$ spectra in Fig. 7 are not completely antisymmetric and symmetric, respectively, due to the small mixing by the spin-orbit interaction $\zeta=H_s/10$.

### D. Intermediate coupling

Comparison of Figs. 6 and 7 shows that there is a strong similarity between the shapes of the $I^1$ spectrum in the limits of $jj$ and $LS$ coupling. For the $I^2$ spectra the low binding-energy peak is similar, but the high binding-energy peak is different, and even forbidden for a pure $j=\frac{1}{2}$ level. The resemblance between the spectra in both coupling limits is due to the fact that spin-up (down) states are always at high (low) binding energy, and that spin-orbit interaction couples the spin and the orbit parallel at low binding energy and antiparallel at high binding energy (cf. Table IV). In the same way, the spectra in intermediate coupling are determined by the spin field and the spin-orbit coupling, therefore, they have similar shapes.

The calculated results for the Fe $3p$ spectra with $\zeta_{3p}=0.95$ and $H_s=1.3$ eV and convoluted with a Lorentzian of 0.6 eV are shown in Fig. 8. The positive

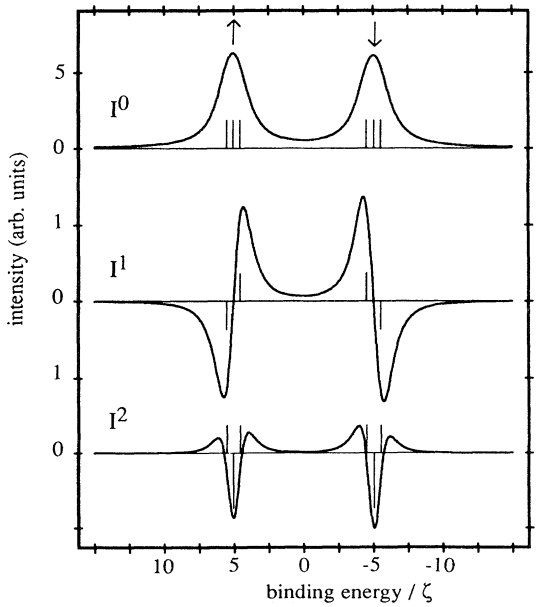


FIG. 7. Calculated $I^x$ spectra of $p$ photoemission for $H_s/\zeta=10$. The spectral weight given by the vertical lines has been convoluted with a Lorentzian of $\Gamma=\zeta$ eV.

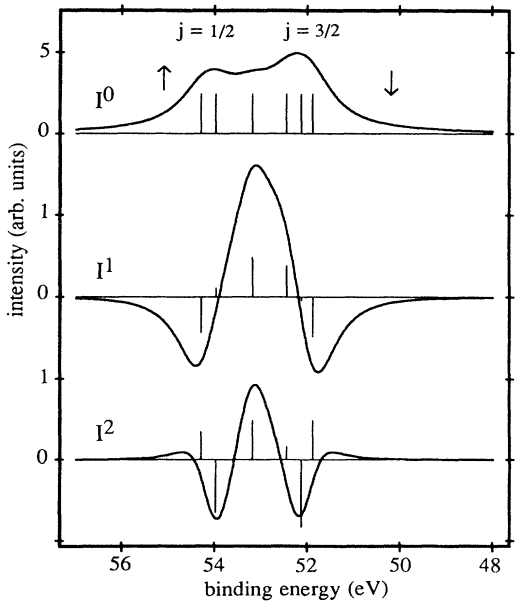


FIG. 8. Calculated $I^x$ spectra of Fe $3p$ photoemission. The spectral weight given by the vertical lines has been convoluted with a Lorentzian of $\Gamma=0.6$ eV.

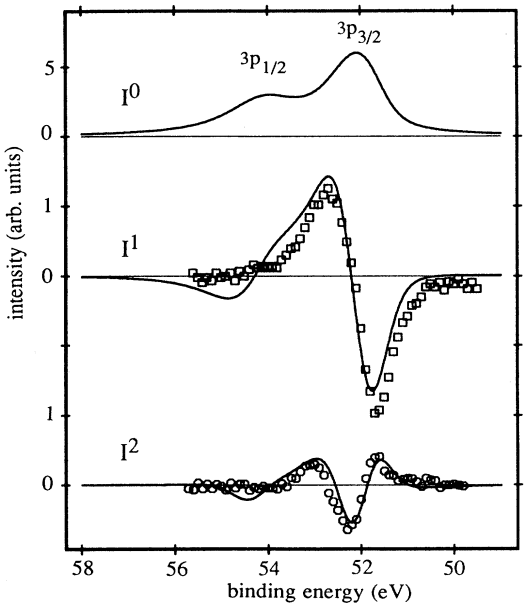


FIG. 9. Calculated $I^x$ spectra of Fe $3p$ photoemission with spin and orbital component dependent linewidth. Experimental MLDAD (squares) and the LD spectrum (circles) from Roth *et al.* (Refs. 2 and 3) on arbitrary intensity scale.

values of $\langle m \rangle$ are located at the high binding-energy side of the $j=\frac{3}{2}$ and at the low binding-energy side of the $j=\frac{1}{2}$ peak, similar to the spectra in the limits of $jj$ and $LS$ coupling. The $I^1$ spectrum shows a $-+$ and $+-$ feature, which are so close together that they form a single $-+-$ structure. The $I^2$ spectrum consists of two $+-+$ features joined together to a single $+-+-+$ structure.

The calculated $I^1$ and $I^2$ spectra in Fig. 8 are in disaccord with the experimental results from Roth *et al.*,[2,3] which are reproduced in Fig. 9. The experimental $I^1$ spectrum has a first statistical moment which is large, whereas that of the theoretical curve is zero (Sec. II E). However, a good agreement can be obtained when we take into account the spin and orbital component dependence of the core hole lifetime (Sec. III F).

### E. Spectral moment analysis

The $n$th moment of the $I^x$ spectrum is defined as

$$I^{x(n)} \equiv \int dE \cdot E^n \cdot I^x(E) \ . \tag{22}$$

The zeroth moment, which is the integrated intensity, is zero for the $I^{x\neq 0}$ spectra. Therefore, the first moment is independent of the absolute binding energy, which makes it a meaningful quantity.

A spin field splits sublevels with different spins such that it does not change the first moment of the spectrum. Since an orbit field gives a linear separation of the sublevels $m$ the first moment of the $I^1$ spectrum will be proportional to the orbit field:

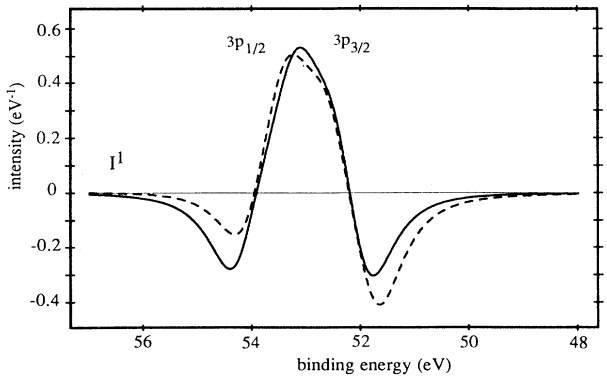


FIG. 10. Calculated $I^1$ spectra of Fe $3p$ photoemission with $\zeta_{3p}=0.95$ eV, $H_s=1.3$ eV, and $H_l=0$ (solid line) and 0.187 eV (dashed line).

$$I^{1(1)}=4H_l \ , \tag{23}$$

where we have normalized to the integrated intensity of the isotropic spectrum, which is equal to the number of electrons in the $l$ shell: $I^{0(0)}=4l+2$. Figure 10 shows the calculated $I^1$ spectrum of the Fe $3p$ core level with and without an orbit field. The dashed line shows the spectrum for $H_l=0.182$, which corresponds to an orbital magnetic moment of $\langle L_z \rangle = -3\mu_B$ for the Hund's rule ground state of a $d^7$ configuration.[24] This gives a first spectral moment of 0.73, in agreement with Eq. (23).

In ferromagnetic iron the valence electrons are strongly delocalized and the orbital magnetic moment of $0.08\mu_B$ is small compared to the Hund's rule ground state. Therefore, the change in $I^{1(1)}$ due to the influence of the orbital magnetization of the valence shell on the core electrons can be neglected. However, in more localized $3d$ materials, such as nickel, the orbital magnetization can give a small effect in the dichroism of the $3p$ photoemission.[7]

### F. Spin and orbital component dependence of the lifetime

So far we have used for all sublevels the same linewidth. However, for shallow core levels the intrinsic line width of the sublevels depends on its spin and orbital components. The spin-up states (majority states) are much broader than the spin-down states (minority states), which is clearly visible in, e.g., the spin-resolved Fe $3s$ photoemission spectrum of iron measured by Hillebrecht, Jungblut, and Kisker.[25] Moreover, atomic calculations show that there is an $LS$-term-dependent lifetime broadening due to configuration interaction and (super) Coster-Kronig decay.[26] Although these effects have no real equivalent in a one-electron model, this does not mean that they are not there. To account for the spin and orbital component dependence of the lifetime, the sublevels were (somewhat arbitrary) convoluted with Lorentzians of the following width: $\Gamma=0.2$ eV for the spin-down state with the lowest binding energy

($m_j=-\frac{3}{2}$); $\Gamma=0.3$ eV for the other spin-down states; $\Gamma=0.9$ eV for the spin-up states. Furthermore, a Gaussian of $\sigma=0.3$ eV was used for the experimental resolution. The $3p$ photoemission spectra for the different spin and light polarizations with these linewidths are shown in Fig. 11. The figure shows the primitive spectra for the $\varepsilon s$ continuum, thus, e.g., from the sublevel $m_j=-\frac{3}{2}$ transitions are allowed with right-circularly polarized light ($\Delta m=1$) but not with left-circularly polarized light ($\Delta m=-1$). The primitive spectra for the $\varepsilon d$ continuum are different, but the fundamental spectra $I^x$ are the same since they are independent of the continuum state [Eq. (3)].

The results for the $I^x$ spectra are shown in Fig. 9. There is an almost perfect agreement with the experimental results for Roth *et al.*[2,3] A small spin dependence of the lifetime is also expected for the $2p$ photoemission in Fig. 6. In both the $2p_{3/2}$ and $2p_{1/2}$ peak the features at the high binding-energy side will then become broader than those at the low binding-energy side.

### G. Spin filtering

Apart from the spin-dependent lifetime broadening, spin-resolved photoemission measurements also indicate the existence of spin-filter effects, i.e., spin-up electrons have a smaller chance to reach the detector than spin-down electrons.[25] The influence of spin filtering on the dichroism is shown in Fig. 12. The $I^1$ spectrum is given separately for spin-up (curve *a*) and spin-down photoemission (curve *b*). Curve *c* gives the dichroism without spin filtering as in Fig. 9, whereas curve *d* is for 30% spin filtering, i.e., the spin-up peaks in the $I^1$ signal have been scaled to 0.7. The change in the first spectral moment is proportional to the amount of spin filtering times the core spin-orbit parameter. Thus although taking into account spin filtering gives a somewhat better agreement between experiment and theory, the overall shape does not change significantly.

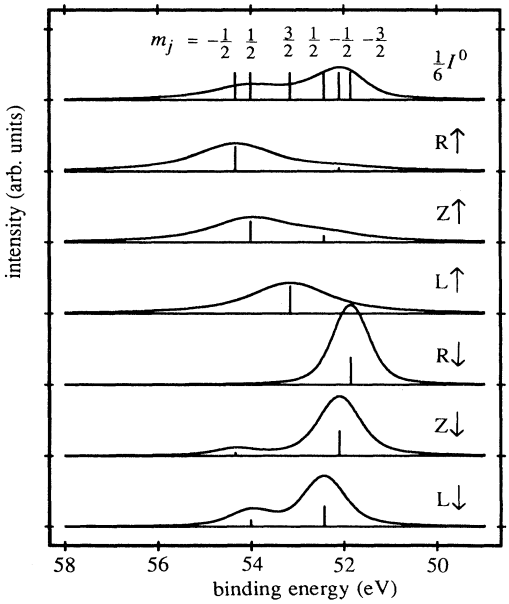


FIG. 11. Calculated Fe $3p$ photoemission spectra to the $\varepsilon s$ continuum for different polarizations of the light and spin with Lorentzian widths of $\Gamma=0.3$ for the spin-down states, except $\Gamma=0.2$ eV for the $m_j=-3/2$, and $\Gamma=0.9$ for the spin-up states, together with a Gaussian convolution of $\sigma=0.3$ eV. The *R*, *Z*, and *L* denote right-circularly ($\Delta m=+1$), *Z*-linearly ($\Delta m=0$), and left-circularly ($\Delta m=-1$) polarized radiation, respectively.

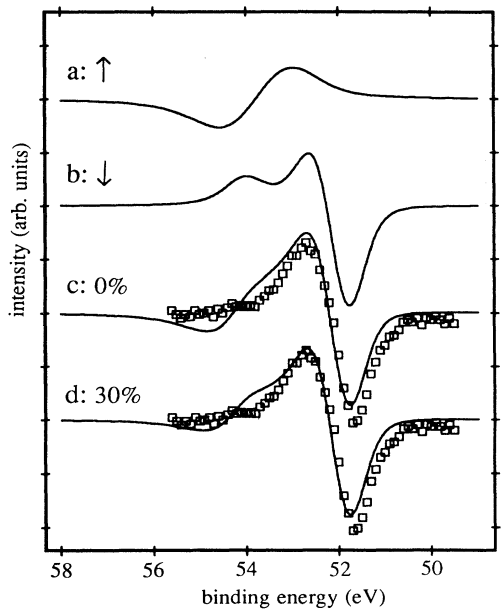


FIG. 12. Calculated $I^1$ spectra for Fe $3p$ photoemission: (a) spin-up, (b) spin-down, (c) without spin filtering, and (d) with 30% spin filtering. Experimental MLDAD spectra (squares) from Roth *et al.* (Ref. 3).

## IV. CONCLUSIONS

In angle-integrated photoemission the light polarization and the induced moment of the atom have the same parity, so that the isotropic and linearly polarized light measure only even magnetic moments, whereas circular polarization measures only odd magnetic moments. However, when the light polarization vector, the *Z* axis of the system (e.g., the molecular axis or the magnetic axis) and the emission direction of the photoelectron are not coplanar, the experimental geometry can be chiral, i.e., the geometry is not a mirror image of itself. Then the interference term between the $l+1$ and $l-1$ channel no longer cancels but depends on the radial matrix elements and the phase difference of these channels and we can measure even magnetic moments with odd polarized light and odd magnetic moments with even polarized light. Thus a spectrum measured in magnetic circular dichroism can also be obtained using linear polarized radiation in a chiral geometry. The advantage is that linear polarization is more easily available and that it might have a more favorable energy dependence than circular

polarization. The physical part can be separated from the angular dependence of the photoemission when the radial matrix elements and the phase factor do not change too strongly over the energy range of the spectrum.

We have explained the influence of the spin-orbit interaction and spin field on the core level dichroism. The shape of the dichroism spectra is determined by $\langle m \rangle$ and $\langle m^2 \rangle$ for each sublevel. The spin-orbit interaction couples this orbital moment (anti)parallel with the prevailing spin-down (up) states at low (high) binding energy. In the limit that the spin field is small compared to the spin-orbit interaction, the magnitude of the dichroism is proportional to the spin field. When the spin field is large compared to the spin-orbit interaction the magnitude of the dichroism is proportional to the spin-orbit interaction.

The calculated Fe $3p$ spectra of metallic iron show a good agreement with the measured data using the Hartree-Fock value of the spin-orbit interaction and the relativistic value of the spin field. An orbit field can change the first spectral moment of the spectrum, but its influence is small for an itinerant system. Spin filtering will also change the first spectral moment, and might be responsible for a reduction in intensity at the high binding-energy side of the peaks. The fine structure of the core level can be resolved by analyzing the dichroism measurements. This can be done more efficiently than in spin-resolved photoemission which in particular suffers from a low count rate. The linewidth shows a strong dependence on the spin and orbital component of the sublevels.

Understanding the results of dichroic photoemission combined with the growing access to synchrotron-radiation devices of intense polarized x rays will bring this technique within reach of the large community of photoelectron spectroscopists. The technique can equally well be applied to magnetically oriented as to nonmagnetic but aligned samples, such as adsorbates on surfaces.

## ACKNOWLEDGMENT

Stimulating discussions with B. T. Thole are gratefully acknowledged.

[1]C. M. Schneider, D. Venus, and J. Kirschner, Phys. Rev. B **45**, 5041 (1992).
[2]Ch. Roth, F. U. Hillebrecht, H. B. Rose, and E. Kisker, Phys. Rev. Lett. **70**, 3479 (1993).
[3]Ch. Roth, F. U. Hillebrecht, H. B. Rose, and E. Kisker, Solid State Commun. **86**, 647 (1993).
[4]L. Baumgarten, C. M. Schneider, H. Petersen, F. Schäfers, and J. Kirschner, Phys. Rev. B **44**, 4406 (1991).
[5]F. U. Hillebrecht and W.-D. Herberg, Z. Phys. B **93**, 299 (1994).
[6]H. Ebert, L. Baumgarten, C. M. Schneider, and J. Kirschner, Phys. Rev. B **44**, 4406 (1991).
[7]G. van der Laan, M. A. Hoyland, M. Surman, C. F. J. Flipse, and B. T. Thole, Phys. Rev. Lett. **69**, 3827 (1992).
[8]G. D. Waddill, J. G. Tobin, and D. P. Pappas, Phys. Rev. B **46**, 552 (1992).
[9]D. Venus, L. Baumgarten, C. M. Schneider, C. Boeglin, and J. Kirschner, J. Phys. Condens. Matter **5**, 1239 (1993).
[10]C. Boeglin, E. Beaurepaire, V. Schorsch, B. Carrière, K. Hricovini, and G. Krill, Phys. Rev. B **48**, 13 123 (1993).
[11]F. Sirotti and G. Rossi, Phys. Rev. B **49**, 15 682 (1994).
[12]G. van der Laan, J. Phys. Condens. Matter **3**, 7443 (1991).
[13]G. van der Laan, Phys. Rev. Lett. **66**, 2527 (1991).
[14]D. Venus, Phys. Rev. B **48**, 6144 (1993); **49**, 8821 (1994).
[15]G. Rossi, F. Sirotti, N. A. Cherepkov, F. Combet Farnoux, and G. Panaccione, Solid State Commun. **90**, 557 (1994).
[16]B. T. Thole and G. van der Laan, Phys. Rev. B **49**, 9613 (1994).
[17]B. T. Thole and G. van der Laan, Phys. Rev. B **44**, 12 424 (1991).
[18]B. T. Thole and G. van der Laan, Phys. Rev. Lett. **70**, 2499 (1993).
[19]G. van der Laan, J. Phys. Soc. Jpn. **63**, 2393 (1994).
[20]R. D. Cowan, *The Theory of Atomic Structure and Spectra* (University of California Press, Berkeley, 1981).
[21]H. Ebert, J. Phys. Condens. Matter **1**, 9111 (1989).
[22]G. van der Laan and I. W. Kirkman, J. Phys. Condens. Matter **3**, 4189 (1992).
[23]G. van der Laan, J. Phys. Condens. Matter **3**, 7443 (1991).
[24]B. T. Thole and G. van der Laan, Phys. Rev. B **50**, 11 474 (1994).
[25]F. U. Hillebrecht, R. Jungblut, and E. Kisker, Phys. Rev. Lett. **65**, 2450 (1990).
[26]K. Okada, A. Kotani, H. Ogasawara, Y. Seino, and B. T. Thole, Phys. Rev. B **47**, 6203 (1993).